Journal of Mathematical Psychology 54 (2010) 322–333

Contents lists available at ScienceDirect

Journal of Mathematical Psychology

journal homepage: www.elsevier.com/locate/jmp

Bounded Ornstein–Uhlenbeck models for two-choice time controlled tasks

Jiaxiang Zhang [a,b,*], Rafal Bogacz [a]

[a] Department of Computer Science, University of Bristol, Bristol BS8 1UB, UK
[b] School of Psychology, University of Birmingham, Birmingham B15 2TT, UK

ARTICLE INFO

Article history:
Received 29 September 2009
Received in revised form
22 February 2010
Available online 26 March 2010

Keywords:
Choice
Decision
Ornstein–Uhlenbeck model
Reflecting boundaries
Absorbing boundaries

ABSTRACT

The Ornstein–Uhlenbeck (O–U) model has been successfully applied to describe the response accuracy and response time in 2-alternative choice tasks. This paper analyses properties and performance of variants of the O–U model with absorbing and reflecting boundary conditions that limit the range of possible values of the integration variable. The paper focuses on choice tasks with pre-determined response time. The type of boundary and the growth/decay parameter of the O–U model jointly determine how the choice is influenced by the sensory input presented at different times throughout the trial. It is shown that the O–U models with two types of boundary are closely related and can achieve the same performance under certain parameter values. The value of the growth/decay parameter that maximizes the accuracy of the model has been identified. It is shown that when the boundaries are introduced, the O–U model may achieve higher accuracy than the diffusion model. This suggests that given the limited range of the firing rates of integrator neurons, the neural decision circuits could achieve higher accuracy employing leaky rather than linear integration in certain tasks. We also propose experiments that could distinguish between different models of choice in tasks with pre-determined response time.

1. Introduction

Making choices on the basis of sensory information is one of the fundamental cognitive functions of intelligent animals. The studies of decision processes in simple 2-alternative forced choice (2AFC) tasks usually employ one of two paradigms. In the time controlled (TC) paradigm, subjects are required to respond immediately after a cue presented at an experimenter-determined time (Dosher, 1976, 1984; Swensson, 1972; Yellott, 1971). Alternatively, in the information controlled (IC) paradigm, subjects are allowed to respond freely whenever they feel confident in their choice (Luce, 1986).

Several mathematical models have been developed over the last half century to describe the behavioural performance as well as the underlying decision process in 2AFC tasks (Busemeyer & Townsend, 1992, 1993; Laming, 1968; Ratcliff, 1978; Ratcliff, Van Zandt, & McKoon, 1999; Stone, 1960; Usher & McClelland, 2001; Vickers, 1970). These sequential sampling models share a common characteristic that the sensory representation of stimuli is accumulated over time to form a choice. Neural correlates of such an accumulation process have been observed in certain cortical areas (Gold & Shadlen, 2002; Kim & Shadlen, 1999; Schall, 2001; Shadlen & Newsome, 2001), which gives further support to the sequential sampling framework.

In the IC paradigm, the decision process depends on the amount of accumulated evidence, i.e., a choice is made as soon as sufficient evidence in favour of one alternative is accumulated. In the TC paradigm, since the time of response is chosen by the experimenter, a choice can be made by simply asking, at the time of response, whether the accumulated evidence supporting the first alternative exceeds that of the second. However, according to such a model for the TC paradigm the accumulated evidence could take arbitrarily large or small values, which could lead to unrealistic predictions (Meyer, Irwin, Osman, & Kounios, 1988). One approach to overcome this problem is to assume that the accumulated evidence is bounded within a certain range (Feller, 1968; Ratcliff, 1988). In our previous study (Zhang, Bogacz, & Holmes, 2009), we compared the effects of two possible boundary mechanisms, reflecting and absorbing boundaries, on a typical sequential sampling model - the diffusion model (Ratcliff, 1978; Ratcliff & McKoon, 2008), and we showed that both boundary types lead to similar performance in the TC paradigm and produce similar fits to experimental data.

This paper extends our previous findings by investigating the dynamics and performance of the Ornstein–Uhlenbeck (O–U) model (Busemeyer & Diederich, 2002; Busemeyer & Townsend, 1992, 1993) with two types of boundaries in the TC paradigm. The O–U model has been successfully applied to a variety of tasks (Diederich, 1995, 1997; Smith, 1995, 2000) and can approximate the same computation carried out by other biologically inspired models (e.g., Usher & McClelland, 2001) in 2AFC tasks. We show that the O–U model with different types of boundaries

* Corresponding author at: School of Psychology, University of Birmingham, Birmingham B15 2TT, UK.
E-mail address: j.zhang.1@bham.ac.uk (J. Zhang).

0022-2496/$ – see front matter © 2010 Elsevier Inc. All rights reserved.
doi:10.1016/j.jmp.2010.03.001

could achieve the same performance under certain parameter values, though the boundaries introduce differential weighting of evidence. We also show that when the boundaries are introduced, the accuracy of the O–U model is higher than that of the diffusion model.

The paper is organized as follows. Section 2 reviews the decision problem and the O–U model as well as boundary mechanisms. Section 3 compares the properties of the O–U models with two types of boundaries. Section 4 investigates the performance of the model and identifies the parameter values that maximize accuracy. Section 5 discusses experimental predictions of the O–U model with boundaries and Section 6 summarizes the implications of our study. Mathematical details are provided in the Appendices. Preliminary results of this study were presented in an abstract form (Zhang & Bogacz, 2006).

2. Sequential sampling models and boundary mechanisms

2.1. Neurobiology of decision

Numerous *in vivo* experiments have been performed to investigate the neural correlates of decision processes in monkeys. In a well-known motion discrimination task used in this line of research, monkeys were instructed to fixate on a random moving dots stimulus presented within a circular aperture (Britten, Shadlen, Newsome, & Movshon, 1993). A proportion of dots move coherently to the left or to the right and the monkey had to respond to the coherent motion direction by making a saccade to a left or right target.

Neural recording data from the motion discrimination task indicate that the decision process involves several cortical regions. First, the neural activity in sensory areas (e.g., the middle temporal (MT) area) has been shown to closely correlate with the statistics of the stimulus (i.e., the motion coherence) (Britten, Newsome, Shadlen, Celebrini, & Movshon, 1996; Britten, Shadlen, Newsome, & Movshon, 1992; Britten et al., 1993). Second, neurons in the lateral interparietal (LIP) area that directly receive inputs from area MT gradually build up or attenuate their activity within a trial (Roitman & Shadlen, 2002; Shadlen & Newsome, 2001). In particular, neural activity in LIP correlates with the direction of eye movements (i.e., the decision) at the time of response. These results suggest that LIP neurons accumulate sensory evidence from area MT to form a choice.

The experimental results indicate that the accumulation of sensory evidence may be a general decision mechanism manifested in different brain regions or species (Gold & Shadlen, 2007; Schall, 2001). Based on this assumption, in this paper we investigate decision problems in 2AFC tasks formalized as follows (Gold & Shadlen, 2001, 2002). Two populations of sensory neurons generate continuous noisy evidence $Y_1(t)$ and $Y_2(t)$ supporting the two alternatives Y_1 and Y_2 at time t. We assume that $Y_1(t)$ and $Y_2(t)$ are normally distributed with constant means μ_1 and μ_2 ($\mu_1, \mu_2 > 0$). The goal of the decision process is to identify which sensory population has the higher mean based on $Y_1(t)$ and $Y_2(t)$.

2.2. The Ornstein–Uhlenbeck model

The Ornstein–Uhlenbeck (O–U) model (Uhlenbeck & Ornstein, 1930) is a stochastic process that was first introduced into psychology by Busemeyer and Townsend (1993). Since then many researchers have applied the O–U model to a variety of studies to account for response accuracy and response time in choice tasks (Busemeyer & Diederich, 2002; Diederich, 1995, 1997; Heath, 1992; Smith, 1995, 1998), and the model has also been extended to multi-alternative tasks (McMillan & Holmes, 2006; Usher & McClelland, 2001).

In the O–U model for 2AFC tasks an imperfect integrator accumulates the difference of sensory evidence supporting two alternatives ($Y_1(t) - Y_2(t)$). Let $X(t)$ denote the value of the integrator state at time t. The O–U model is described by the following stochastic differential equation:

$$dX(t) = (\lambda X(t) + \mu)\, dt + \sigma\, dW, \tag{1}$$

where μ and σ denote the mean and standard deviation of the normally distributed quantity $Y_1(t) - Y_2(t)$ (i.e., $\mu = \mu_1 - \mu_2$), $dX(t)$ denotes the increment of evidence over a small unit of time dt, $dW(t)$ is Gaussian white noise with mean zero and unit variance, and λ is a growth/decay parameter. According to the decision problem proposed above, the sign of μ determines the correct choice. More specifically, $\mu > 0$ implies that the first alternative Y_1 is correct ($\mu_1 > \mu_2$), and $\mu < 0$ implies that the second alternative Y_2 is correct ($\mu_1 < \mu_2$). For simplicity, we hereafter set $\mu > 0$ in this paper. The magnitude of μ and σ determine the task difficulty, i.e., for $|\mu|$ close to zero or large σ, it is difficult to distinguish which alternative (Y_1 or Y_2) has higher mean. On each trial, the decision process starts at $t = 0$ with a starting point $X_0 = X(0) = 0$. In the IC paradigm, the integrator continuously accumulates evidence according to Eq. (1) until $X(t)$ reaches a decision threshold. In the TC paradigm, the decision process terminates at a pre-determined time t_c, and the choice is made on the basis of the final integrator state $X(t_c)$, i.e., the model selects Y_1 if $X(t_c) > 0$, or Y_2 if $X(t_c) < 0$. Throughout this paper we focus on the TC paradigm and quantify the model's performance by the error rate $P(t_c)$, which is the probability of making an incorrect choice when the response is required at time t_c. The expression for the error rate of the O–U model is given by Busemeyer and Townsend (1993):

$$P(t_c) = \Phi\left(-\frac{\mu}{\sigma}\sqrt{\frac{2\left(e^{\lambda t_c}-1\right)}{\lambda\left(e^{\lambda t_c}+1\right)}}\right), \tag{2}$$

$$\text{where } \Phi(u) = \int_{-\infty}^{u} \frac{1}{\sqrt{2\pi}} e^{-\frac{v^2}{2}}\, dv. \tag{3}$$

It is worth noting that the parameter λ affects the linear drift rate $\lambda X(t) + \mu$, and as a result the O–U model with nonzero λ exhibits differential weighting of evidence within a trial. That is, for $\lambda > 0$ the evidence presented early in a trial has a larger influence on the decision (a primacy effect), and for $\lambda < 0$ the choice mainly depends on the evidence presented later in a trial (a recency effect) (Wallsten & Barton, 1982). An explicit proof of this property is available in Busemeyer and Townsend (1993). In particular, for $\lambda = 0$, the weighting of evidence is independent of the time of its presentation and the O–U model simplifies to a diffusion model (Ratcliff, 1978; Ratcliff & McKoon, 2008). In Section 3 we will investigate how the primacy and recency effects of the O–U model are affected by boundaries.

2.3. Boundary mechanisms

In earlier versions of sequential sampling models, the value of the integrator states was unconstrained. As mentioned in the Introduction, this type of model allows the integrator state to have arbitrarily large or small values. This is, however, a simplification. First, it is not realistic that any biological system could represent an infinite amount of evidence. Second, when accumulated evidence is not limited, a sequential sampling model may not fit experimental data (Ratcliff, 1988). One way to eliminate the above problems is to transform the integrator state through a nonlinear activation function[1] (Brown et al., 2005; Brown & Holmes, 2001; Usher & McClelland, 2001). Another approach, the

[1] In fact, the O–U process can be obtained from a nonlinear transformation of the Wiener process (Cox & Miller, 1965, p. 229; Smith, in press).

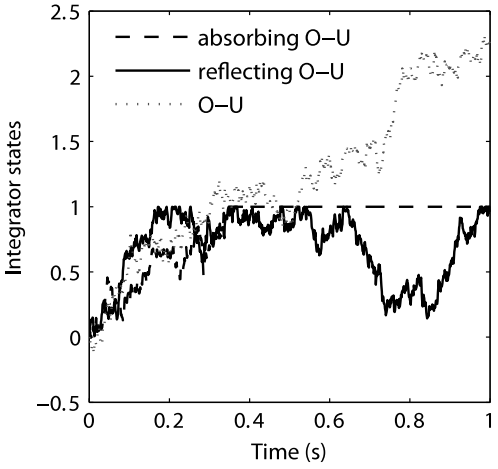

Fig. 1. Examples of trajectories of the O–U models with absorbing boundary (dashed line), reflecting boundary (solid line), and without boundary (dotted line). Models were simulated with $\mu = 0.5$ s^{-1}, $\lambda = 1$, $\sigma = 1$ s^{-1}, $dt = 0.001$ s, and boundaries $b = 1$.

focus of this paper, is to apply boundary conditions to the existing linear models, which provides an approximation of the nonlinear activation functions (Usher & McClelland, 2001).

The first boundary mechanism is the absorbing boundary (Feller, 1968), which was originally applied to choice tasks in which IC and TC paradigms were intermixed (i.e. the subjects were instructed to respond freely on some trials, or after a timed cue on other trials) (Diederich & Busemeyer, 2003; Ratcliff, 1988; Ratcliff & Rouder, 2000). Once the integrator hits an absorbing boundary, the accumulation process terminates and the integrator state is maintained afterwards. To introduce absorbing boundaries to the O–U model, we assume two symmetric boundaries at $\pm b$, and then, the O–U model with absorbing boundaries can be described by:

$$\begin{cases} X(t+dt) = b, & \text{if } X(t) + dX(t) \geq b \text{ or } X(t) = b, \\ X(t+dt) = -b, & \text{if } X(t) + dX(t) \leq -b \\ & \quad \text{or } X(t) = -b, \\ X(t+dt) = X(t) + dX(t), & \text{otherwise,} \end{cases} \tag{4}$$

where $dX(t)$ is given by Eq. (1). In the TC paradigm, the choice is determined by which boundary the integrator hits first, or if neither boundary is reached before t_c, the choice is determined by the same rule as the one used for the model without boundaries (see Section 2.2).

The second boundary mechanism is the reflecting boundary (Zhang et al., 2009) (also see Diederich, 1995; Diederich & Busemeyer, 2003; Ratcliff & Smith, 2004), which only restricts the amount of accumulated evidence that can be represented by the integrator. In other words, the value of the integrator state cannot exceed a reflecting boundary, but it may continue to change (i.e., move back) due to noise, as specified by:

$$\begin{cases} X(t+dt) = b, & \text{if } X(t) + dX(t) \geq b, \\ X(t+dt) = -b, & \text{if } X(t) + dX(t) \leq -b, \\ X(t+dt) = X(t) + dx(t), & \text{otherwise.} \end{cases} \tag{5}$$

Hereafter we refer to the O–U model with absorbing and reflecting boundaries as absorbing O–U and reflecting O–U models, and the model without a boundary as the unbounded O–U model. Fig. 1 shows sample paths of integrator states in the O–U models with both types of boundaries, compared with the unbounded O–U model. For the absorbing O–U model, the choice can be determined early in a trial (after 0.35 s in Fig. 1). For the reflecting O–U model, the preferred choice may change throughout the decision process until the end of the trial.

In a previous study, we compared the boundary effects on one sequential sampling model — the diffusion model (Zhang et al., 2009). We showed that the diffusion model with two types of boundaries produce exactly the same error rate for any given t_c. Moreover, the absorbing and reflecting boundaries yield a primacy and recency effect, respectively. In the next section we will show that similar properties also hold for the bounded O–U model.

2.4. Optimal decision making theory

Due to evolutionary pressure, neural systems are likely to adapt to their environment and optimize their behaviour to achieve desired goals (Anderson, 1990). This assumption has been invoked in the study of perceptual decision making, and it has been proposed that the brain may implement statistically optimal decision-making procedures (Bogacz, 2007, 2009; Bogacz et al., 2006; Gold & Shadlen, 2001, 2002, 2007). In the sequential sampling framework, an optimal decision procedure would achieve the lowest error rate and shortest response time compared with all possible procedures to integrate sensory evidence[2]. For the TC paradigm, the optimal procedure is the one that yields the lowest error rate for any given response time.

Recall that the decision problem proposed in Section 2.1 is to identify which of the two alternatives has higher mean inputs. This problem can be converted to the problem of hypothesis testing in statistics (Ghosh, 1970; Lehmann, 1959), and the optimal procedure satisfying the above criterion is provided by the Neyman and Pearson (NP) procedure. It has been proved that among all hypothesis tests, the NP procedure minimizes the overall probability of accepting the false hypothesis for fixed sample size (Neyman & Pearson, 1933), and therefore it minimizes the error rate for any response time. Bogacz et al. (2006) showed that as the time intervals between samples approach zero, the NP procedure becomes equivalent to the diffusion model. Hence, the diffusion model is the optimal decision procedure in the TC paradigm in the Neyman–Pearson sense. Since the O–U model with $\lambda = 0$ can be reduced to the diffusion model, the O–U model also maximizes accuracy when $\lambda = 0$. In Section 4, we will show that this is no longer the case for the bounded O–U model.

3. Properties of bounded O–U models

3.1. Dynamics of bounded O–U models

The dynamics of the absorbing and reflecting O–U models can be illustrated by the probability density $p(X, t)$ of the integrator states $X(t)$ at time t, which is calculated in Appendix A by solving the Kolmogorov backward equation with boundary conditions. The density function $p(X, t)$ of bounded O–U models is a weighted sum of an infinite series:

$$p(X, t) = \sum_{j=0}^{\infty} e^{-\xi_j t} K_j(X) \phi_j(X_0), \tag{6}$$

where $K_j(X)$ is defined in Eq. (A.16). ξ_j are the non-negative eigenvalues from Eqs. (A.27) and (A.30), and $\phi_j(X_0)$ are the associated eigenfunctions defined in Eqs. (A.26) and (A.29) as a function of the starting point X_0. The eigenvalues and eigenfunctions depend on the type of boundaries. There exist infinitely many eigenvalues that can be found numerically, and an approximation of $p(X, t)$ can

[2] The optimality criterion for the IC paradigm is to consider which decision strategy yields the fastest response time for any given error rate. The procedure that satisfies this criterion is provided by the Sequential Probability Ratio Test (Barnard, 1946; Wald, 1947).

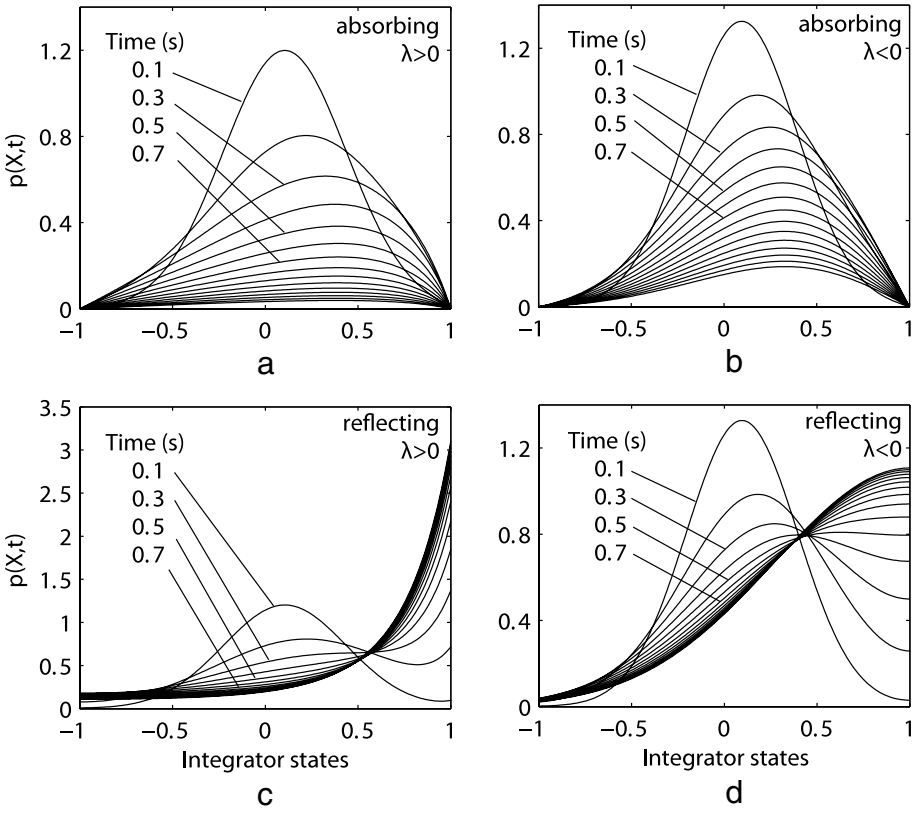

Fig. 2. Probability densities of integrator states in the bounded O–U models. State values of the integrator are shown on horizontal axes. Densities are shown for parameters $\mu = \sigma = 1$ s^{-1}, and $b = 1$. For each panel, different curves show densities at different time instants from 0.1 s to 2 s. The density functions $p(X, t)$ are calculated in Appendix A with eigenvalues shown in Table 1. All solutions start at $X_0 = 0$. (a) The absorbing O–U model with $\lambda = 1$. (b) The absorbing O–U model with $\lambda = -1$. (c) The reflecting O–U model with $\lambda = 1$. (d) The reflecting O–U model with $\lambda = -1$.

be obtained by taking a partial sum of finite terms. The more eigenvalues included in Eq. (6), the more accurate the approximation of the density function $p(X, t)$.

Fig. 2 compares the probability densities of the absorbing and reflecting O–U models at several time instants. During the first hundred milliseconds, all densities are close to a Gaussian distribution with mean close to the starting point X_0 and shifted towards the upper boundaries as time grows. For large t, the density of the absorbing O–U model collapses to zero, while the reflecting O–U model has nonzero equilibrium distributions, with a small proportion to the left of the origin, corresponding to the probability of making an incorrect choice (for $\mu > 0$).

The difference between the stationary densities can be explained from the expression of $p(X, t)$. For any $\xi_j > 0$, the time-dependent coefficient $e^{-\xi_j t}$ in Eq. (6) monotonically decreases and converges to zero as t grows. Table 1 shows the first ten eigenvalues ξ_j. For the absorbing O–U model all eigenvalues are positive, hence the density of the absorbing O–U model converges to $p(X, t) = 0$ as $t \to \infty$. For the reflecting O–U model, one of the eigenvalues is equal to zero $\xi_0 = 0$, hence the density $p(X, t)$ converges to $K_0(X)\phi_0(X_0)$ as $t \to \infty$. It is also interesting to note that the eigenvalues ξ_j $(j > 0)$ of the absorbing and reflecting O–U models are symmetric by flipping the sign of λ.

3.2. Primacy and recency effects

Previous studies showed that differential weighting of evidence (i.e., the primacy and recency effects) can be introduced by either the parameter λ of the unbounded O–U model (Busemeyer & Townsend, 1993) or two types of boundaries (Zhang et al., 2009). Here we investigate the primacy and recency effects in the O–U models by applying the reverse correlation method. We simulate the unbounded, absorbing, and reflecting O–U models, each with positive and negative λ values. For each model considered, the time course of sensory evidence is recorded and averaged only from trials resulting in correct choices. The averaged evidence represents how the model weights noisy inputs during the decision process. For $\mu > 0$, the model makes correct decisions if the integrated evidence is positive at the end of a trial. Hence a larger averaged input from correct trials indicates that the sensory input at that time point has, on average, a large influence on the final choice, and a smaller averaged input indicates that the choice depends to a lesser extent on the input at that time.

Table 1
Eigenvalues of the bounded O–U models with positive and negative λ. The eigenvalues are numerically obtained by seeking the roots of the Eqs. (A.27) and (A.30). The parameters of the bounded O–U models are $\mu = \sigma = 1$ s^{-1}, and $b = 1$.

j	Absorbing		Reflecting	
	$\lambda = -1$	$\lambda = 1$	$\lambda = -1$	$\lambda = 1$
0	–	–	0	0
1	1.26	2.26	2.26	1.26
2	5.08	6.08	6.08	5.08
3	11.27	12.27	12.27	11.27
4	19.90	20.90	20.90	19.90
5	31.01	32.01	32.01	31.01
6	44.58	45.58	45.58	44.58
7	60.62	61.62	61.62	60.62
8	79.12	80.12	80.12	79.12
9	100.10	101.10	101.10	100.10
10	123.54	124.54	124.54	123.54

The simulation results are shown in Fig. 3. First, positive and negative λ values introduce primacy (Fig. 3a) and recency (Fig. 3d) effects to the unbounded O–U model, which is consistent

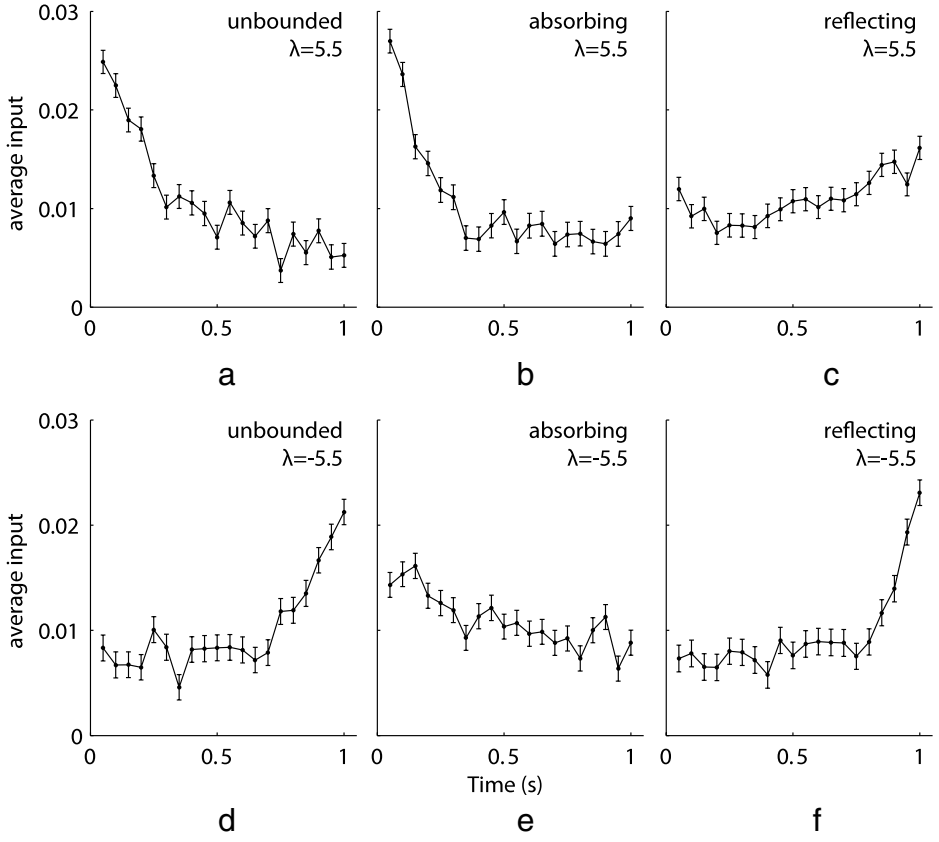

Fig. 3. Primacy and recency effects for the bounded and unbounded O–U models with positive λ (top panels) and negative λ (bottom panels). In each panel the O–U model is simulated for 10,000 trials. For all correct trials the input to the O–U model at every time step is recorded and averaged. The data points show the mean of the inputs and the error bars show the standard error. In all panels the parameter values are $\mu = 0.71\ s^{-1}$, $\sigma = 1\ s^{-1}$, $b = 0.47$, $t_c = 1$s. (a) The unbounded O–U model with $\lambda = 5.5$. (b) The absorbing O–U model with $\lambda = 5.5$. (c) The reflecting O–U model with $\lambda = 5.5$. (d) The unbounded O–U model with $\lambda = -5.5$. (e) The absorbing O–U model with $\lambda = -5.5$. (f) The reflecting O–U model with $\lambda = -5.5$.

with theoretical predictions by Busemeyer and Townsend (1993). Second, the absorbing O–U model exhibits a strong primacy effect for $\lambda > 0$ (Fig. 3b), but no clear effect was observed for $\lambda < 0$ (Fig. 3e). By contrast, a positive λ value does not produce a clear effect in the reflecting O–U model (Fig. 3c), but the reflecting O–U model has a strong recency effect for $\lambda < 0$ (Fig. 3f).

Therefore, the primacy/recency effect in the bounded O–U models is jointly determined by two independent elements: the value of λ and the type of the boundary. Given different combinations of the two elements, the primacy/recency effect in the bounded O–U model is maintained if λ and the boundary provide the same effects (Figs. 3b and 3f). On the other hand, the joint effect is weakened if λ and the boundary introduces opposite effects, as shown in Figs. 3c and 3e. By appropriately setting the two parameters the joint primacy/recency effects introduced by the boundary and λ could cancel each other. In Section 4.2 we show that this condition leads to the optimal performance of the bounded O–U model.

4. Performance of bounded O–U models

4.1. The error rate of bounded O–U models

For the reflecting O–U model, since the density of the integrator $p(X, t)$ has unit mass (see Fig. 2), the error rate is equal to the proportion of $p(X, t)$ that lies on the 'error' side of the origin, i.e., if $\mu > 0$, the error rate of the reflecting O–U model can be calculated by integrating the density $p(X, t)$ from $-b$ to 0:

$$P_{(\mathrm{ref})}(t_c) = \int_{-b}^{0} p(X, t_c)\, dX, \tag{7}$$

where "ref" stands for reflecting boundary. Therefore by estimating $p(X, t)$ numerically we can obtain an approximation of the error rate. For the absorbing O–U model, such a calculation is not available as $p(X, t)$ converges to zero as t grows.

Now let us compare the error rates of the O–U models with two types of boundaries. For the unbounded O–U model, the error rate remains the same if we flip the sign of λ (see Eq. (2)). Fig. 4 shows the error rates of the bounded O–U models with positive and negative λ at different t_c. The result suggests that there exists an error rate symmetry in the bounded O–U models. That is, by flipping the sign of λ, the absorbing and reflecting O–U models produce the same error rate for any t_c. This relationship can be represented as:

$$P_{(\mathrm{abs})}(t_c, -\lambda) = P_{(\mathrm{ref})}(t_c, \lambda), \tag{8}$$

where $P_{(\mathrm{abs})}(.)$ and $P_{(\mathrm{ref})}(.)$ denote the error rates of the absorbing and reflecting O–U models with parameters specified in the brackets. We have not succeeded in giving a complete proof of Eq. (8) since an analytical expression for the error rate of the bounded O–U model is not available. However we are able to prove a special case of Eq. (8) when $t_c \to \infty$, which is given in Appendix B.

In summary, the absorbing and reflecting O–U models with opposite signs of λ produce the same accuracy, and thus they would provide the same fit to data from experiments in the TC paradigm.

4.2. The optimal parameter

In the TC paradigm, the unbounded O–U model achieves the minimum error rate when $\lambda = 0$ (i.e., when it reduces to the

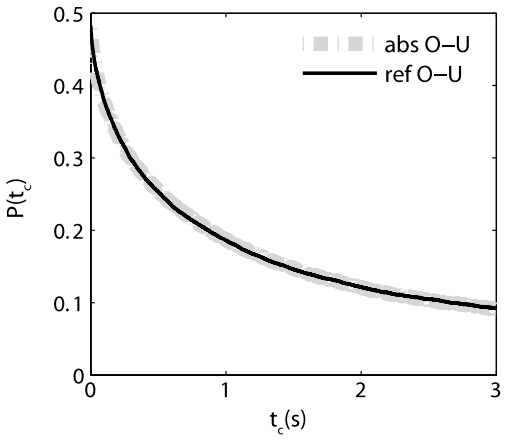

Fig. 4. The error rate of the bounded O–U models at different t_c. The models were simulated with parameters: $\mu = \sigma = 1$ s^{-1} and $b = 1$. Every data point is averaged from 100,000 trials. The reflecting O–U model (solid line) is simulated with $\lambda = 2$, and the absorbing O–U model (dashed line) is simulated with $\lambda = -2$.

diffusion model) (Bogacz et al., 2006 and also see Section 2.4). After introducing boundaries, an intriguing question arises: is $\lambda = 0$ still the optimal parameter value for the bounded O–U models? If not, what is the optimal λ value that yields the lowest error rate for the bounded O–U models?

To answer this question, we simulate the bounded O–U models with different parameter values. The error rates of the bounded O–U models with different values of λ, b and t_c are shown as contour plots in Fig. 5. The result suggests that the bounded O–U models with $\lambda = 0$ are not always optimal, but the optimal value of λ depends on the values of other parameter such as b and t_c. First, if b is relatively small ($b < 0.2$ in Fig. 5), the value of λ does not significantly affect the performance of the bounded O–U models in all panels of Fig. 5. This result is expected, since if the interval between the two boundaries is tiny, the integrator state is restricted to be around X_0, and in this case the noise would dominate the choice process. Therefore, the models produce large error rates (around 40%) in this region. Second, if b is sufficiently large ($b > 2$ in Fig. 5), the integrator hardly reaches any of the boundaries before t_c used in the simulation, and hence the bounded O–U models are approximately equivalent to the unbounded O–U model, in which $\lambda = 0$ gives the lowest error rate for any t_c.

Except for these two extreme parameter regions, the error rate is affected by the values of λ, b and t_c. In general, given b and t_c, for the absorbing O–U model, $\lambda < 0$ gives the best performance,

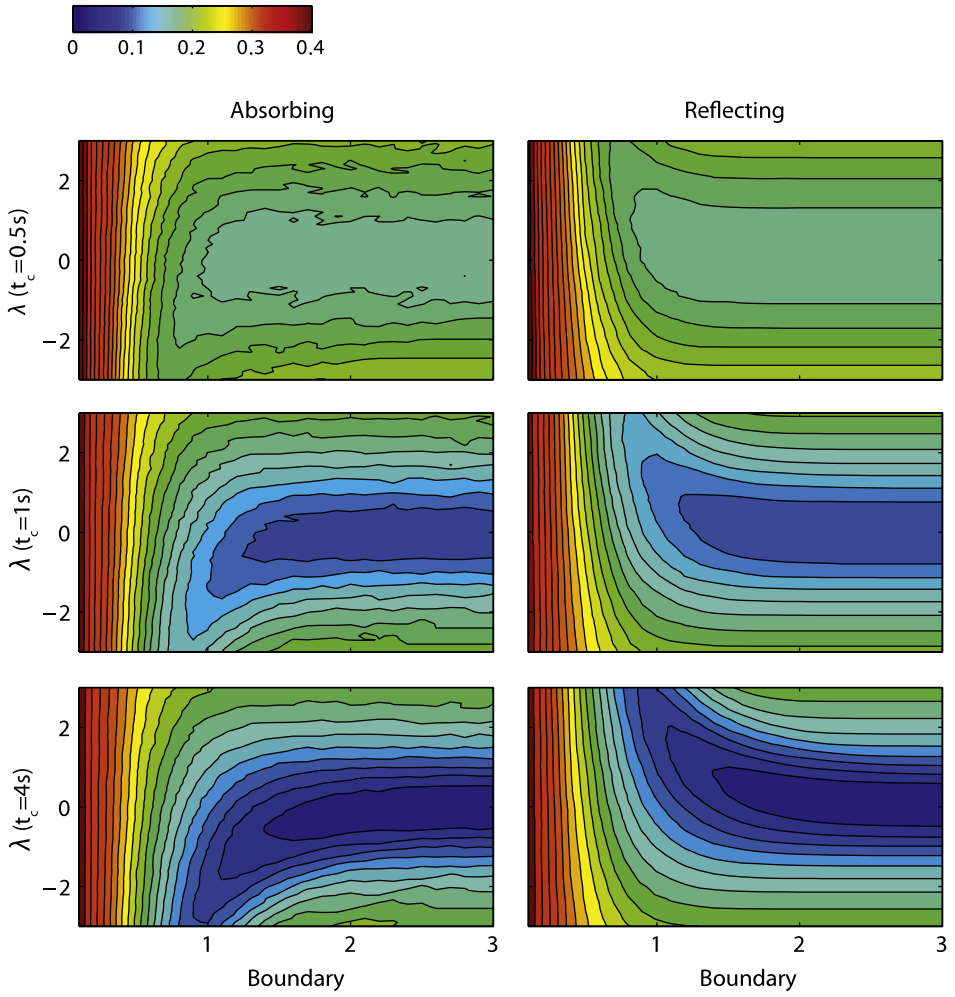

Fig. 5. The contour plots of the error rates of the bounded O–U models with different parameter values. The bounded O–U models are simulated with the following parameters: λ in $[-3,3]$ with step 0.1, b in $[0.1,3]$ with step 0.1, $\mu = \sigma = 1$ s^{-1}, and $t_c = 0.5$s, 1 s, and 4 s. For each possible combination of the parameter values, the absorbing and reflecting O–U models are simulated for 10,000 trials to obtain the mean error rates. The error rates are then grouped by the value of t_c and the type of boundaries, and illustrated as contour plots. The horizontal axes show the value of b, and the vertical axes show the value of λ. Each contour plot has 20 contour levels and the colormaps are the same for all panels. Left panels show the error rates of the absorbing O–U model, and right panels show the error rates of the reflecting O–U model. The panels in each row show the plots that have the same value of t_c, as indicated on the vertical axes.

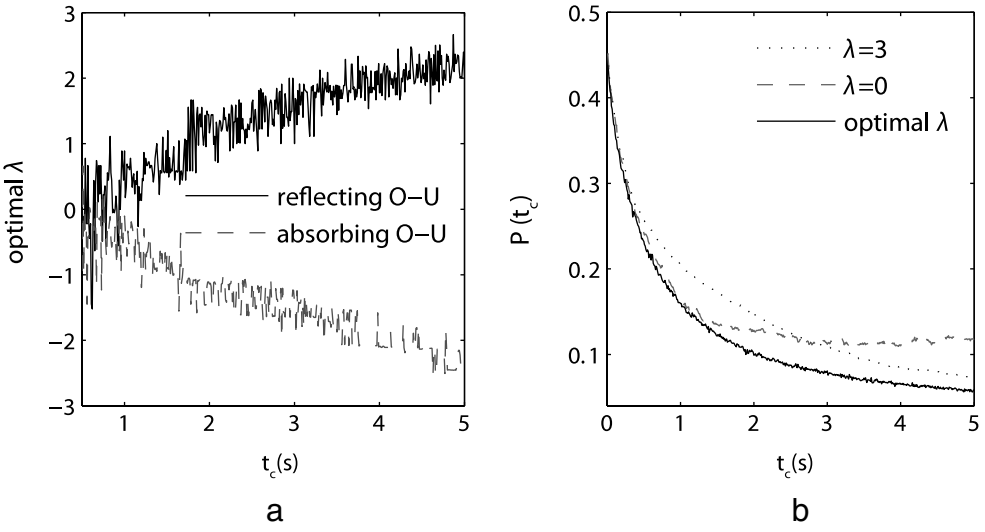

Fig. 6. Optimal performance of the bounded O–U models. (a) The optimal λ values of reflecting and absorbing O–U models for different t_c varying from 0.5s to 10s (in steps of 0.01 s). For each t_c, the absorbing and reflecting O–U models are simulated with parameters $\mu = \sigma = 1$ s^{-1}, $b = 1$, and λ varying from −100 to 100. For each value of λ the model is simulated for 10,000 trials, and the λ that yields minimum error rate is recorded as the optimal value at t_c. (b) Error rates of the reflecting O–U model at different t_c. The model is simulated with the same parameters (μ, σ, b) as in panel (a). Dotted line shows the error rate of the model with $\lambda = 3$. Dashed line shows the error rate of the model with $\lambda = 0$ (i.e., the diffusion model). Solid line shows the error rate of the model with optimal λ values from panel (a). Each data point is averaged over 10,000 trials.

while for the reflecting O–U model, $\lambda > 0$ yields the minimum error rate. This optimal value of λ is consistent with the joint primacy/recency effects of the bounded O–U models proposed in Section 3.2. Recall that the recency effect introduced by the reflecting boundary can be weakened by setting $\lambda > 0$, and vice versa. To achieve the optimal performance, the primacy/recency effects of the boundaries and λ should be balanced and cancelled, so that the sensory evidence from different time points contribute equally to the choice, as in the optimal NP decision procedure (i.e., no primacy/recency effects). The simulation results in Fig. 5 accord with this hypothesis.

Fig. 5 also shows that for fixed b, the absolute value of λ that yields the optimal performance increases when extending t_c, i.e., the optimal λ increases for the reflecting O–U model and decreases for the absorbing O–U model. To find the optimal λ values, we simulate the bounded O–U model under different t_c. For each t_c, we numerically found the value of λ that yields the minimum error rate, and the results are shown in Fig. 6a. For the reflecting O–U model, the optimal λ increases as t_c increases, with decreasing slope. The optimal λ for the absorbing O–U model is a mirror of that for the reflecting O–U model, which decreases as t_c grows. This result further supports the error rate symmetry of the bounded O–U models (Eq. (8)), because if a specific λ value is optimal for the reflecting O–U model, $-\lambda$ would be optimal for the absorbing O–U model.

To validate the optimality of λ values in Fig. 6a, we simulated the reflecting O–U model with different t_c. For each t_c, λ is set to be the optimal value shown in Fig. 6a. For comparison, we also simulated the reflecting O–U model with fixed λ values $\lambda = 3$ and $\lambda = 0$. The error rates of the three models are illustrated in Fig. 6b. The bounded O–U model with optimal λ values achieves lower error rates than the model with other constant λ.

We also show in Appendix C that the error rates of the bounded O–U model with optimal λ do not decrease to 0 as $t \to \infty$. Thus the model is consistent with an observation that the error rates of human subjects in the TC paradigm do not decrease to 0 as t increases on difficult trials (Usher & McClelland, 2001).

5. Experimental predictions

The two types of boundaries may characterize different subjects' behaviour in psychological experiments. The absorbing boundary can account for the behaviour in which the choice is made before the end of the trial and never changed. The reflecting boundary may imply that the subjects hesitate between the two choices even when sufficient evidence is available, and may change their preference later in the trial. Nevertheless, due to the error rate symmetry, it is not trivial to differentiate between the two types of boundary on the basis of experimental data from simple 2AFC tasks, as the absorbing and reflecting O–U models (with opposite sign of λ) would always produce the same fit.

To investigate primacy and recency effects in the TC paradigm, stimuli could be used that differ in the information they contain at different times after stimulus onset (Huk & Shadlen, 2005; Usher & McClelland, 2001). For example, in the motion discrimination task (see Section 2.1) the coherence of motion can be increased for a short period on each trial (Usher, Tsetsos, & Teodorescu, 2009). The primacy effect would be present, if such an increase in coherence had the highest influence on accuracy when occurring after stimulus onset. The recency effect would be present, if the increase had the highest influence before the response. Note however, that such an experiment cannot differentiate between the absorbing O–U model with negative λ and the reflecting O–U model with positive λ, because neither model predicts strong primacy or recency effects. Our analysis suggests that these two models maximize accuracy, and given evolutionary pressure for accuracy of decisions, we predict that one of these two models should describe choices in the TC paradigm with long t_c.

We propose that the absorbing O–U model with negative λ and the reflecting O–U model with positive λ could be distinguished in a motion discrimination experiment in which the coherence is manipulated in a similar way to that recently proposed by Zhou, Wong-Lin, and Holmes (2009). In particular, the coherence could be increased by a strong pulse c_1 for an interval of length t_1, and then decreased by a smaller amount $c_2 < c_1$ for a longer interval $t_2 > t_1$ (Fig. 7a). If the parameters of the perturbation

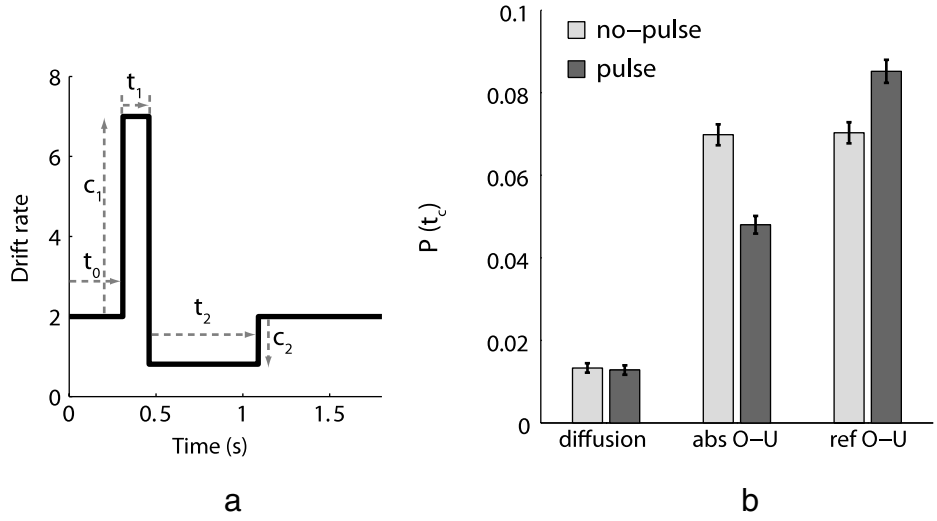

Fig. 7. The decision task with pulse perturbation. (a) The drift rate with pulse perturbation. The parameter values are: $\mu = 2\ s^{-1}$, $c_1 = 5\ s^{-1}$, $c_2 = 1.19\ s^{-1}$, $t_0 = 310$ ms, $t_1 = 150$ ms, $t_2 = 630$ ms. (b) The error rate of the absorbing and reflecting O–U models, compared with that of the unbounded diffusion model. The models were simulated with parameter values: $b = 0.7$, $\lambda = \pm 5$ (-5 for the absorbing O–U model and 5 for the reflecting O–U model), $c = 2\ s^{-1}$, and $t_c = 1.8$ s. Light grey bars show the error rate of the models with constant drift rate $\mu = 2\ s^{-1}$, and dark grey bars show the error rate of the models with time-varying drift rate from (a). The error bars show the standard error from 10,000 trials.

satisfied $c_1t_1 = c_2t_2$, the average motion coherence in a trial would remain unchanged (hence the unbounded diffusion model predicts that such a perturbation would have no effect on accuracy). The absorbing O–U model with negative λ predicts that such a perturbation would increase accuracy, because the first pulse could cause the correct absorbing boundary to be reached. By contrast, the reflecting O–U model with positive λ predicts that the perturbation would decrease accuracy, because the information in the first pulse may be lost if the reflecting boundary is reached. Fig. 7b verifies these predictions by simulations. Note that the effects of the pulse perturbation are not due to the primacy/recency properties of the models (as we intentionally selected the boundary and λ values so that the primacy/recency effects were balanced), but originate from the characteristics of the two types of boundaries. However, it is worth mentioning that the effect of the pulse only occurs if the following two conditions are satisfied. First, the pulse needs to be sufficiently large to move the integrator to the boundary. Second, the pulse needs to be presented early in a trial. Otherwise the pulse will not affect the performance of the absorbing O–U model (as the inputs do not affect the decision process once the integrator hits absorbing boundaries).

Our analysis also shows that the accuracy in the TC paradigm is maximized if parameter λ is adapted[3] depending on the required reaction time t_c. If subjects indeed adapt λ depending on t_c, then they should achieve higher accuracy when t_c can be anticipated. This predicts that the accuracy for a given t_c should be higher when t_c is constant within a block (and hence can be anticipated) than when it varies within a block.

6. Discussion

The present study compared the properties and performance of the O–U models with absorbing and reflecting boundaries in the TC paradigm. The main results are summarized in Table 2. First, we showed how different boundaries affect the dynamics of the decision process by visualizing the probability density of the integrator state (Fig. 2). We then showed that the primacy and recency effects introduced by the boundaries and the parameter λ coexist in the bounded O–U models, and the joint effects depend on the two independent elements (Fig. 3). Moreover, the absorbing and reflecting O–U models can achieve the same error rate for any t_c by flipping the sign of λ (Fig. 4). Finally, we showed that the reflecting O–U model with positive λ (and the absorbing O–U model with negative λ) produces lower error rates than the model with $\lambda = 0$ (Fig. 5), and we numerically found the optimal λ values for the bounded O–U models that yield the minimum error rate (Fig. 6).

Table 2
Comparison of the properties of the absorbing and reflecting O–U models.

		Absorbing	Reflecting
Weighting of inputs	$\lambda > 0$	Uniform	Recency
	$\lambda < 0$	Primacy	Uniform
	$\lambda = 0$	Primacy	Recency
Error rate	$\lambda \neq 0$	Symmetric	
	$\lambda = 0$	Equality	
Optimality		$\lambda < 0$	$\lambda > 0$

6.1. Optimal integration with boundaries

This paper has shown that when the range of possible values of the integrator state is constrained, the simple integration of difference in evidence is not the optimal procedure, and a better performance can be yield by the O–U model, especially for long t_c. This suggests that given the limited range of the firing rates of integrator neurons, the neural decision circuits could achieve a higher accuracy in tasks with long t_c employing an integration procedure similar to the O–U model rather than the linear integration. In particular, if the brain employs a mechanism similar to the absorbing boundaries, as suggested by the neurophysiological data of Kiani, Hanks, and Shadlen (2008), the accuracy of choices in tasks with long t_c would be maximized by employing leaky integration.

[3] In the TC paradigm the O–U model produces the same simulated behaviour as a neurocomputational model called the leaky competing accumulator (LCA) model (Usher & McClelland, 2001), when the λ parameter of the O–U model is set to the difference between two parameters of the LCA model: synaptic weights of inhibitory connections and leak. Therefore, the effective value of λ can be adapted by changing the inhibitory weights in the LCA model. In the biological neural networks synaptic weights can be adapted either via synaptic plasticity or through neuromodulation.

6.2. Relationship to other studies

Since the O–U model is reduced to the diffusion model when $\lambda = 0$, the results presented in this paper extend our previous findings on the diffusion model with boundaries (Zhang et al., 2009). In particular, Zhang et al. (2009) showed that the diffusion models with absorbing and reflecting boundaries achieve the same error rate. Such equality is a special case of the error rate symmetry of the bounded O–U models by setting $\lambda = -\lambda = 0$.

In the TC paradigm, the O–U model produces the same simulated behaviour as the leaky competing accumulator (LCA) model (Usher & McClelland, 2001), when the λ parameter of the O–U model is set to the difference between inhibition and decay parameters of the LCA model. Simulations of the LCA model with attracting boundaries showed that it maximizes the accuracy in the TC paradigm when the inhibition is lower than the leak (Bogacz, Usher, Zhang, & McClelland, 2007). These simulations are consistent with the results of this paper, because for such parameter values the LCA model corresponds to the O–U model with $\lambda < 0$.

Acknowledgments

This work was supported by the ORS grant and the EPSRC grant EP/C514416/1. We thank Eric Shea-Brown for discussion on the asymptotic error rate of the bounded O–U model.

Appendix A. The probability density function for the bounded O–U model

This appendix describes calculation of the probability density function $p(X, t)$ for the O–U models with absorbing and reflecting boundary conditions. A solution of this problem for $\lambda < 0$ has been provided by Saphores (2005). Here we reiterate the calculation and extend the solution to both positive and negative λ.

Let us consider a general case: an O–U process defined in Eq. (1) is bounded over $[L, R]$, where L and R are finite absorbing or reflecting boundaries defined in Eqs. (4) and (5), respectively. Let $p(X, X_0, t)$ be the probability density of $X(t)$ at time t given that $X(0) = X_0$. The density satisfies the Kolmogorov backward equation (Karlin & Taylor, 1981):

$$\frac{\partial p(X, X_0, t)}{\partial t} = -(\mu + \lambda X_0)\frac{\partial p(X, X_0, t)}{\partial X_0} + \left(\frac{\sigma^2}{2}\right)\frac{\partial^2 p(X, X_0, t)}{\partial X_0^2}, \tag{A.1}$$

where the coefficients μ, λ, and σ are defined in Eq. (1). Since $X(t)$ has fixed value X_0 at $t = 0$, the initial probability distribution is a delta function:

$$p(X, X_0, 0) = \delta(X - X_0). \tag{A.2}$$

Goel and Dyn (2003) showed that if boundaries are absorbing, $p(X, X_0, t)$ has to satisfy:

$$p(X, X_0, t) = 0, \quad \text{for } X_0 = L \text{ or } R, \tag{A.3}$$

and reflecting boundaries at L and R imply the following no-flux boundary conditions:

$$\frac{\partial p(x, y, t)}{\partial y} = 0, \quad \text{for } X_0 = L \text{ or } R. \tag{A.4}$$

To solve Eq. (A.1) we separate variables (Boyce & DiPrima, 1997) and seek a solution as the weighted sum of elementary solutions.

$$p(X, X_0, t) = \sum_{j=0}^{\infty} a_j(t)\,\phi_j(X_0). \tag{A.5}$$

For one of the elementary solutions $a(t)\,\phi(X_0)$, substituting Eq. (A.5) in (A.1) and rearranging terms, we obtain:

$$\frac{a'(t)}{a(t)} = \frac{\sigma^2}{2\phi(X_0)}\phi''(X_0) + \frac{\mu + \lambda X_0}{\phi(X_0)}\phi'(X_0). \tag{A.6}$$

Since the left side of Eq. (A.6) depends only on t, while the right side only on X_0, they must be equal to some constant, denoted by $-\xi$. Then the solution for the time-dependent coefficients $a(t)$ is:

$$a(t) = Ke^{-\xi t}, \tag{A.7}$$

and the function $\phi(X_0)$ satisfies:

$$\frac{\sigma^2}{2}\phi''(X_0) + (\mu + \lambda X_0)\phi'(X_0) + \xi\phi(X_0) = 0. \tag{A.8}$$

Substituting (A.7) into (A.5), the density $p(X, X_0, t)$ yields:

$$p(X, X_0, t) = \sum_{j=0}^{\infty} K_j\, e^{-\xi_j t}\,\phi_j(X_0). \tag{A.9}$$

The coefficients K_j in Eq. (A.9) are obtained from the initial probability at $t = 0$. Firstly multiply both sides of (A.8) by a function of X_0:

$$r(X_0) = \frac{2}{\sigma^2}\exp\left(\frac{2\mu X_0 + \lambda X_0^2}{\sigma^2}\right), \tag{A.10}$$

then $\phi(X_0)$ should satisfy

$$\begin{aligned}&\exp\left(\frac{2\mu X_0 + \lambda X_0^2}{\sigma^2}\right)\phi''(X_0) + \frac{2\mu + 2\lambda X_0}{\sigma^2}\\ &\quad\times \exp\left(\frac{2\mu X_0 + \lambda X_0^2}{\sigma^2}\right)\phi'(X_0) + \xi r(X_0)\phi(X_0)\\ &= \left[\exp\left(\frac{2\mu X_0 + \lambda X_0^2}{\sigma^2}\right)\phi'(X_0)\right]' + \xi r(X_0)\phi(X_0) = 0.\end{aligned} \tag{A.11}$$

Eq. (A.11) is the classical Sturm–Liouville equation. From the Sturm–Liouville theorem (Boyce & DiPrima, 1997), there exists an infinite set of non-negative eigenvalues ξ_j $(j = 1, 2, \ldots)$, and associated eigenfunctions $\phi_j(X_0)$ that satisfy Eq. (A.11). Besides, the normalized eigenfunctions form an orthogonal set with respect to the function $r(X_0)$. Hence for any two eigenfunctions $\phi_i(X_0)$ and $\phi_j(X_0)$, there is

$$\frac{\int_L^R r(X_0)\phi_j(X_0)\phi_i(X_0)\,dX_0}{\int_L^R r(X_0)\phi_j^2(X_0)\,dX_0} = \delta_{ij}, \tag{A.12}$$

where δ_{ij} is the Kronecker delta function. For $t = 0$, a single elementary solution of the density $p(X, X_0, t)$ in Eq. (A.5) is:

$$p(X, X_0, t) = K_j\phi_j(X_0) = \delta(X - X_0). \tag{A.13}$$

Multiplying both sides of Eq. (A.13) by:

$$\frac{r(X_0)\phi_i(X_0)}{\int_L^R r(X_0)\phi_j^2(X_0)\,dX_0}, \tag{A.14}$$

and taking the integral over the interval $[L, R]$, we obtain:

$$K_j\frac{\int_L^R r(X_0)\phi_j(X_0)\phi_i(X_0)\,dX_0}{\int_L^R r(X_0)\phi_j^2(X_0)\,dX_0} = \frac{\int_L^R r(X_0)\phi_i(X_0)\delta(X - X_0)\,dX_0}{\int_L^R r(X_0)\phi_j^2(X_0)\,dX_0}, \tag{A.15}$$

and the coefficient K_j is:

$$K_j = \frac{r(X)\phi_j(X)}{\int_L^R r(X_0)\phi_j^2(X_0)\,dX_0}. \tag{A.16}$$

To get the solutions of eigenvalues ξ and eigenfunctions $\phi(X_0)$, we need to solve the differential equation (A.8). First assume $\lambda < 0$, and define a new variable z:

$$z = \sqrt{-2\lambda}\,\frac{X_0 + \mu/\lambda}{\sigma}. \tag{A.17}$$

Substituting Eq. (A.17) into (A.8) yields:

$$\lambda\phi''(z) - \lambda z\phi'(z) - \xi\phi(z) = 0. \tag{A.18}$$

We seek the solution of $\phi(z)$ of the form:

$$\phi(z) = e^{z^2/4}\omega(z). \tag{A.19}$$

Substituting Eq. (A.19) in (A.18), the exponential term is canceled and the new function is:

$$\frac{d^2\omega(z)}{dz^2} + \left(\frac{1}{2} - \frac{\xi}{\lambda} - \frac{1}{4}z^2\right)\omega(z) = 0. \tag{A.20}$$

Eq. (A.20) is the classical parabolic cylinder function, and there exists two independent solutions, given by (Abramowitz & Stegun, 1965):

$$\begin{cases} \omega_1(z) = \exp\left(\frac{1}{4}z^2\right)\,\mathcal{F}\left(\frac{\xi}{2\lambda};\ \frac{1}{2};\ \frac{z^2}{2}\right), \\ \omega_2(z) = z\exp\left(\frac{1}{4}z^2\right)\,\mathcal{F}\left(\frac{1}{2} + \frac{\xi}{2\lambda};\ \frac{3}{2};\ \frac{z^2}{2}\right), \end{cases} \tag{A.21}$$

where $\mathcal{F}(.)$ is the confluent hypergeometric function. Substituting Eq. (A.21) in (A.19) and representing Eq. (A.21) as a function of X_0 yields:

$$\begin{cases} E_1(X_0) = \mathcal{F}\left(\frac{\xi}{2\lambda};\ \frac{1}{2};\ -\frac{\lambda}{\sigma^2}(X_0 + \mu/\lambda)^2\right), \\ E_2(X_0) = \sqrt{-2\lambda}\,\frac{X_0+\mu/\lambda}{\sigma}\,\mathcal{F}\left(\frac{1}{2} + \frac{\xi}{2\lambda};\ \frac{3}{2};\ -\frac{\lambda}{\sigma^2}(X_0 + \mu/\lambda)^2\right). \end{cases} \tag{A.22}$$

For the case of $\lambda > 0$, select the substitution of X_0 as:

$$z = \sqrt{2\lambda}\,\frac{X_0 + \mu/\lambda}{\sigma}. \tag{A.23}$$

Then by following the same approach, we can obtain the elementary solutions for $\phi(X_0)$:

$$\begin{cases} E_1(X_0) = \exp\left(-\frac{(\mu + \lambda X_0)^2}{\lambda\sigma^2}\right) \\ \qquad \times\,\mathcal{F}\left(\frac{1}{2} - \frac{\xi}{2\lambda};\ \frac{1}{2};\ \frac{\lambda}{\sigma^2}(X_0 + \mu/\lambda)^2\right), \\ E_2(X_0) = \exp\left(-\frac{(\mu + \lambda X_0)^2}{\lambda\sigma^2}\right) \\ \qquad \times\,\mathcal{F}\left(1 - \frac{\xi}{2\lambda};\ \frac{3}{2};\ \frac{\lambda}{\sigma^2}(X_0 + \mu/\lambda)^2\right). \end{cases} \tag{A.24}$$

The solution of Eq. (A.8) is the linear combination of the two elementary solutions given by (A.22) or (A.24) (depending on the sign of λ). For absorbing boundaries, $\phi(X_0)$ must satisfy the following boundary condition (cf. Eqs. (A.3) and (A.5)):

$$\phi(L) = \phi(R) = 0. \tag{A.25}$$

By appropriately selecting the weighting value, the solution of $\phi(X_0)$ for absorbing boundary condition is:

$$\phi(X_0) = E_1(X_0)E_2(L) - E_1(L)E_2(X_0), \tag{A.26}$$

and the eigenvalues ξ can be obtained numerically by seeking the roots of the equation:

$$E_1(L)E_2(R) - E_1(R)E_2(L) = 0. \tag{A.27}$$

If the boundaries are reflecting, the boundary condition changes to:

$$\frac{\partial\phi(L)}{\partial X_0} = \frac{\partial\phi(R)}{\partial X_0} = 0. \tag{A.28}$$

The above condition is satisfied when:

$$\phi(X_0) = E_1(X_0)E_2'(L) - E_1'(L)E_2(X_0), \tag{A.29}$$

and the associated eigenvalues are the roots of:

$$E_1'(L)E_2'(R) - E_1'(R)'E_2'(L) = 0. \tag{A.30}$$

Substituting Eqs. (A.16) and (A.26) (or (A.29) for reflecting boundaries) in (A.9), we obtain a series representation of $p(X, t)$ with starting point X_0.

Appendix B. Symmetry of the error rate for the bounded O–U model

Since the analytical solution of the error rate of the bounded O–U model is not available, it is not straightforward to prove the symmetry property of the bounded O–U model in Eq. (8) for arbitrary t_c. Instead, this appendix proves a special case of Eq. (8) when $t_c \to \infty$, i.e., the target equation is:

$$P_{(\text{abs})}(t_c, \lambda)|_{t_c\to\infty} = P_{(\text{ref})}(t_c, -\lambda)|_{t_c\to\infty}. \tag{B.1}$$

First let us consider the absorbing O–U model bounded between $\pm b$. To simplify the calculation, we make the following transformation:

$$\hat{b} \leftarrow \frac{b}{\mu}, \quad \text{and} \quad \hat{\mu} \leftarrow \left(\frac{\mu}{\sigma}\right)^2. \tag{B.2}$$

For the absorbing O–U model, since the density of the integrator state $p(X, t)$ converges to zero as t_c grows, $X(t)$ will reach one of the boundaries as $t_c \to \infty$. Hence, the error rate of the absorbing O–U model with infinite t_c is the same as the error rate of the unbounded O–U model in the IC paradigm, which has an analytical solution given by (Bogacz et al., 2006):

$$P_{(\text{abs})}(t_c, \lambda)|_{T_c\to\infty} = \frac{\text{erf}\left(\sqrt{\frac{\hat{\mu}}{\lambda}}(1 + \lambda\hat{b})\right) - \text{erf}\left(\sqrt{\frac{\hat{\mu}}{\lambda}}\right)}{\text{erf}\left(\sqrt{\frac{\hat{\mu}}{\lambda}}(1 + \lambda\hat{b})\right) - \text{erf}\left(\sqrt{\frac{\hat{\mu}}{\lambda}}(1 - \lambda\hat{b})\right)}, \tag{B.3}$$

where erf(.) is the error function given by:

$$\text{erf}(x) = \frac{2}{\sqrt{\pi}}\int_0^x e^{-t^2}\,dt. \tag{B.4}$$

Now let us consider the error rate of the reflecting O–U model. Recall that the reflecting O–U model has zero eigenvalue $\xi_0 = 0$ (cf. Table 1). For $t_c \to \infty$, the time-dependent coefficients $e^{-\xi t}$ in Eq. (A.9) vanish and the stationary density of $X(t)$ is:

$$p(X, +\infty) = \phi_0(X_0)\frac{r(X)\phi_0(X)}{\int_{-b}^{b} r(X_0)\phi_0^2(X_0)\,dX_0}, \tag{B.5}$$

where $r(X)$ is defined in Eq. (A.10), and the eigenfunction ϕ_0 is defined in Eq. (A.29).

For $\lambda < 0$, the two elementary solutions of Eq. (A.29) are given by Eq. (A.22). In order to simplify the expression, let:

$$V = \frac{X}{\hat{\mu}} + \frac{1}{\lambda}, \quad \text{and} \quad V_0 = \frac{X_0}{\hat{\mu}} + \frac{1}{\lambda} = \frac{1}{\lambda}, \tag{B.6}$$

and the lower and upper boundaries in Eq. (A.22) are given by:

$$L = \frac{1}{\lambda} - \hat{b}, \quad \text{and} \quad R = \frac{1}{\lambda} + \hat{b}. \tag{B.7}$$

By this transformation, the drift term μ in Eq. (1) is eliminated and the density $p(X, +\infty)$ can be calculated in the terms of V and V_0:

$$p(V, +\infty) = \phi_0(V_0)\frac{r(V)\phi_0(V)}{\int_L^R r(V_0)\phi_0^2(V_0)\,dV_0}. \tag{B.8}$$

Substituting Eqs. (A.6) and (A.7) in Eq. (A.22), and setting the eigenvalue $\xi_0 = 0$, the two elementary solutions of the eigenfunction $\phi_0(w)$ become:

$$\begin{cases} E_1(V) = \mathcal{F}\left(0;\ \frac{1}{2};\ -\hat{\mu}\lambda V^2\right), \\ E_2(V) = V\sqrt{-2\hat{\mu}\lambda}\ \mathcal{F}\left(\frac{1}{2};\ \frac{3}{2};\ -\hat{\mu}\lambda V^2\right). \end{cases} \tag{B.9}$$

The derivative of Eq. (B.9) is:

$$\begin{cases} E_1'(V) = 0, \\ E_2'(V) = \sqrt{-2\hat{\mu}\lambda}\ \exp(\hat{\mu}\lambda V^2). \end{cases} \tag{B.10}$$

Substituting Eqs. (B.9) and (B.10) in (A.29) yields the eigenfunction of the stationary distribution:

$$\phi_0(V) = \sqrt{-2\hat{\mu}\lambda}\exp\left(-\frac{\hat{\mu}}{\lambda}(\lambda\hat{b}-1)^2\right). \tag{B.11}$$

Recall that the error rate of the reflecting O–U model can be represented by integrating $p(V, t_c)$ from the lower boundary L to the start point V_0 (cf. Eq. (7)). For $t_c \to \infty$, $p(V, t_c)$ converges to the stationary distribution in Eq. (B.8). Hence the error rate is:

$$P_{(\mathrm{ref})}(t_c, -\lambda)|_{t_c\to\infty} = \phi_0(V_0)\frac{\int_L^{V_0} r(V)\phi_0(V)\,dV}{\int_L^R r(V_0)\phi_0^2(V_0)\,dV_0}. \tag{B.12}$$

Substituting Eqs. (A.10) and (B.11) in (B.12), the error rate can be analytically obtained, as:

$$P_{(\mathrm{ref})}(t_c, \lambda)|_{t_c\to\infty} = \frac{\mathrm{erfi}\left(\sqrt{\frac{\hat{\mu}}{\lambda}}\right) + \mathrm{erfi}\left(\sqrt{\frac{\hat{\mu}}{\lambda}}(-1+\lambda\hat{b})\right)}{\mathrm{erfi}\left(\sqrt{\frac{\hat{\mu}}{\lambda}}(-1+\lambda\hat{b})\right) + \mathrm{erfi}\left(\sqrt{\frac{\hat{\mu}}{\lambda}}(1+\lambda\hat{b})\right)}, \tag{B.13}$$

where erfi(.) is the imaginary error function, given by:

$$\mathrm{erfi}(z) = \mathrm{erf}(zi)/i, \tag{B.14}$$

where i is the imaginary unit. Substituting Eq. (B.14) in (B.13), the ER of the reflecting O–U model is:

$$P_{(\mathrm{ref})}(t_c, \lambda)|_{t_c\to\infty} = \frac{\mathrm{erf}\left(\sqrt{\frac{\hat{\mu}}{-\lambda}}(1+(-\lambda)\hat{b})\right) - \mathrm{erf}\left(\sqrt{\frac{\hat{\mu}}{-\lambda}}\right)}{\mathrm{erf}\left(\sqrt{\frac{\hat{\mu}}{-\lambda}}(1+(-\lambda)\hat{b})\right) + \mathrm{erf}\left(\sqrt{\frac{\hat{\mu}}{-\lambda}}(1-(-\lambda)\hat{b})\right)}. \tag{B.15}$$

For $\lambda > 0$, the two elementary solutions in Eq. (A.29) are given by Eq. (A.24). By applying the same approach as (B.6)–(B.10), the eigenfunction now becomes:

$$\phi_0(V) = \sqrt{2\hat{\mu}\lambda}\exp\left(-\frac{\hat{\mu}}{\lambda}(\lambda\hat{b}-1)^2\right). \tag{B.16}$$

Substituting Eqs. (A.10) and (B.16) in (B.12), the eigenfunction has the same expression as Eq. (B.15). Therefore Eq. (B.15) satisfies both positive and negative λ.

Comparing Eqs. (B.3) and (B.15), it is clear that when the sign of λ in the two equations changes, the error rates of the absorbing and reflecting O–U models are exactly the same. i.e., the bounded O–U model satisfies Eq. (B.1).

Appendix C. The asymptotic approximation of the error rate for the bounded O–U model

This appendix derives the asymptotic error rate of the bounded O–U model with the optimal value of λ in the limit of $t \to \infty$. For the absorbing O–U model, the simulation result suggests that the error rate for $t \to \infty$ monotonically decreases as λ ($\lambda < 0$) decreases (cf. Fig. 6). Hence the asymptotic error rate $P(\infty, \lambda)$ is given by Eq. (B.3) as $\lambda \to -\infty$. Substituting Eq. (B.14) in (B.3) we have:

$$P(\infty, \lambda)|_{\lambda\to-\infty} = \frac{1}{1 + \lim_{\lambda\to-\infty}\frac{\mathrm{erfi}\left(\sqrt{\frac{\hat{\mu}}{\lambda}}(\lambda\hat{b}-1)\right)}{\mathrm{erfi}\left(\sqrt{\frac{\hat{\mu}}{\lambda}}(\lambda\hat{b}+1)\right)}}. \tag{C.1}$$

Recall the asymptotic expansion of the complementary error function for large x:

$$\mathrm{erfi}(x) = \frac{e^{-x^2}}{\sqrt{\pi}x}\left(1 - \frac{1}{2x^2} + \frac{3}{4x^4} - \cdots\right). \tag{C.2}$$

This gives:

$$\frac{\mathrm{erfi}\left(\sqrt{\frac{\hat{\mu}}{\lambda}}(\lambda\hat{b}-1)\right)}{\mathrm{erfi}\left(\sqrt{\frac{\hat{\mu}}{\lambda}}(\lambda\hat{b}+1)\right)} = e^{4\hat{\mu}\hat{b}}\left(1 + 2\hat{\mu}\hat{b}\lambda + \frac{2\hat{b}(\hat{\mu}\hat{b}-1)}{\hat{\mu}}\lambda^2\right) + O(\lambda^3). \tag{C.3}$$

Substituting Eq. (C.3) in (C.1) we have:

$$P(\infty, \lambda)|_{\lambda\to-\infty} = \frac{1}{1+e^{4\hat{\mu}\hat{b}}} = \frac{1}{1+e^{\frac{4\mu b}{\sigma^2}}}. \tag{C.4}$$

Note that we could obtain the same result for the reflecting O–U model as $\lambda \to \infty$.

It is interesting to note that for the bounded diffusion model the error rate is equal to (Zhang et al., 2009):

$$P(\infty, 0) = \frac{1}{1+e^{\frac{2\mu b}{\sigma^2}}}. \tag{C.5}$$

Comparing Eqs. (C.4) and (C.5) reveals that the bounded O–U model can achieve the accuracy for $t \to \infty$ that would be obtained by the bounded diffusion model with twice as distant boundaries.

References

Abramowitz, M., & Stegun, I. A. (1965). *Handbook of mathematical functions with formulas, graphs and mathematical tables*. New York: Dover.

Anderson, J. R. (1990). *The adaptive character of thought*. Hillsdale, NJ: Lawrence Erlbaum.

Barnard, G. A. (1946). Sequential tests in industrial statistics. *Journal of the Royal Statistical Society*, *8*(1), 1–26.

Bogacz, R. (2007). Optimal decision making theories: linking neurobiology with behaviour. *Trends in Cognitive Sciences*, *11*(3), 118–125.

Bogacz, R. (2009). Optimal decision making theories. In J.-C. Dreher, & L. Tremblay (Eds.), *Handbook of reward and decision making* (pp. 375–397).

Bogacz, R., Brown, E., Moehlis, J., Hu, P., Holmes, P., & Cohen, J. D. (2006). The physics of optimal decision making: a formal analysis of models of performance in two-alternative forced choice. *Psychological Review*, *113*(4), 700–765.

Bogacz, R., Usher, M., Zhang, J., & McClelland, J. L. (2007). Extending a biologically inspired model of choice: multi-alternatives, nonlinearity and value-based multidimensional choice. *Philosophical Transactions of the Royal Society, Series B*, *362*, 1655–1670.

Boyce, W. E., & DiPrima, R. C. (1997). *Elementary differential equations and boundary value problems* (6th ed.). New York: Wiley.

Britten, K. H., Newsome, W. T., Shadlen, M. N., Celebrini, S., & Movshon, J. A. (1996). A relationship between behavioral choice and the visual responses of neurons in macaque mt. *Visual Neuroscience*, *13*(1), 87–100.

Britten, K. H., Shadlen, M. N., Newsome, W. T., & Movshon, J. A. (1992). The analysis of visual motion: a comparison of neuronal and psychophysical performance. *Journal of Neuroscience*, *12*(12), 4745–4765.

Britten, K. H., Shadlen, M. N., Newsome, W. T., & Movshon, J. A. (1993). Responses of neurons in macaque mt to stochastic motion signals. *Visual Neuroscience*, *10*(6), 1157–1169.

Brown, E., Gao, J., Holmes, P., Bogacz, R., Gilzenrat, M., & Cohen, J. D. (2005). Simple neural networks that optimize decisions. *International Journal of Bifurcation and Chaos*, *15*(3), 803–826.

Brown, E., & Holmes, P. (2001). Modeling a simple choice task: stochastic dynamics of mutually inhibitory neural groups. *Stochastics and Dynamics*, *1*(2), 159–191.

Busemeyer, J. R., & Diederich, A. (2002). Survey of decision field theory. *Mathematical Social Sciences*, *43*(3), 345–370.

Busemeyer, J. R., & Townsend, J. T. (1992). Fundamental derivations from decision field theory. *Mathematical Social Sciences*, *23*(3), 255–282.
Busemeyer, J. R., & Townsend, J. T. (1993). Decision field theory: a dynamic-cognitive approach to decision making in an uncertain environment. *Psychological Review*, *100*(3), 432–459.
Cox, D. R., & Miller, H. D. (1965). *The theory of stochastic processes*. London, UK: Chapman and Hall.
Diederich, A. (1995). Intersensory facilitation of reaction time: evaluation of counter and diffusion coactivation models. *Journal of Mathematical Psychology*, *39*(2), 197–215.
Diederich, A. (1997). Dynamic stochastic models for decision making under time constraints. *Journal of Mathematical Psychology*, *41*(3), 260–274.
Diederich, A., & Busemeyer, J. (2003). Simple matrix methods for analyzing diffusion models of choice probability, choice response time, and simple response time. *Journal of Mathematical Psychology*, *47*(3), 304–322.
Dosher, B. A. (1976). The retrieval of sentences from memory: a speed-accuracy study. *Cognitive psychology*, *8*(3), 291–310.
Dosher, B. A. (1984). Discriminating preexperimental (semantic) from learned (episodic) associations: a speed-accuracy study. *Cognitive psychology*, *16*(4), 519–555.
Feller, W. (1968). *An introduction to probability theory and its applications*. New York: Wiley.
Ghosh, B. K. (1970). *Sequential tests of statistical hypotheses*. Addison-Wesley Educational Publishers.
Goel, N., & Dyn, N. (2003). *Stochastic models in biology*. Caldwell, NJ: Blackburn Press.
Gold, J. I., & Shadlen, M. N. (2001). Neural computations that underlie decisions about sensory stimuli. *Trends in Cognitive Sciences*, *5*(1), 10–16.
Gold, J. I., & Shadlen, M. N. (2002). Banburismus and the brain: decoding the relationship between sensory stimuli, decisions and reward. *Neuron*, *36*(2), 299–308.
Gold, J. I., & Shadlen, M. N. (2007). The neural basis of decision making. *Annual Review of Neuroscience*, *30*, 535–574.
Heath, R. A. (1992). A general nonstationary diffusion model for two-choice decision-making. *Mathematical Social Sciences*, *23*(3), 283–310.
Huk, A. C., & Shadlen, M. N. (2005). Neural activity in macaque parietal cortex reflects temporal integration of visual motion signals during perceptual decision making. *Journal of Neuroscience*, *25*(45), 10420–10436.
Karlin, S., & Taylor, H. M. (1981). *A second course in stochastic processes*. New York: Academic Press.
Kiani, R., Hanks, T. D., & Shadlen, M. N. (2008). Bounded integration in parietal cortex underlies decisions even when viewing duration is dictated by the environment. *Journal of Neuroscience*, *28*(12), 3017–3029.
Kim, J. N., & Shadlen, M. N. (1999). Neural correlates of a decision in the dorsolateral prefrontal cortex of the macaque. *Nature Neuroscience*, *2*, 176–185.
Laming, D. R. J. (1968). *Information theory of choice reaction time*. New York: Wiley.
Lehmann, E. L. (1959). *Testing statistical hypotheses*. New York: Wiley.
Luce, R. D. (1986). *Response times and their role in inferring elementary mental organization*. New York: Oxford University Press.
McMillan, T., & Holmes, P. (2006). The dynamics of choice among multiple alternatives. *Journal of Mathematical Psychology*, *50*(1), 30–57.
Meyer, D. E., Irwin, D. E., Osman, A. M., & Kounios, J. (1988). The dynamics of cognition and action: mental processes inferred from speed-accuracy decomposition. *Psychological Review*, *95*(2), 183–237.
Neyman, J., & Pearson, E. S. (1933). On the problem of the most efficient tests of statistical hypotheses. *Philosophical Transactions of the Royal Society of London, Series A*, *231*, 289–337.
Ratcliff, R. (1978). A theory of memory retrieval. *Psychological Review*, *85*(2), 59–108.
Ratcliff, R. (1988). Continuous versus discrete information processing: modeling accumulation of partial information. *Psychological Review*, *95*(2), 238–255.
Ratcliff, R., & Rouder, J. N. (2000). A diffusion model account of masking in two-choice letter identification. *Journal of Experimental Psychology: Human Perception & Performance*, *26*(1), 127–140.
Ratcliff, R., & Smith, P. L. (2004). A comparison of sequential sampling models for two-choice reaction time. *Psychology Review*, *111*(2), 333–367.
Ratcliff, R., & McKoon, G. (2008). The diffusion decision model: theory and data for two-choice decision tasks. *Neural Computation*, *20*(4), 873–922.
Ratcliff, R., Van Zandt, T., & McKoon, G. (1999). Connectionist and diffusion models of reaction time. *Psychology Review*, *106*(2), 261–300.
Roitman, J. D., & Shadlen, M. N. (2002). Response of neurons in the lateral intraparietal area during a combined visual discrimination reaction time task. *Journal of Neuroscience*, *22*(21), 9475–9489.
Saphores, J. D. (2005). The density of bounded diffusions. *Economics Letters*, *86*(1), 87–93.
Schall, J. D. (2001). Neural basis of deciding, choosing and acting. *Nature Reviews Neuroscience*, *2*, 33–42.
Shadlen, M. N., & Newsome, W. T. (2001). Neural basis of a perceptual decision in the parietal cortex (area lip) of the rhesus monkey. *Journal of Neurophysiology*, *86*(4), 1916–1936.
Smith, P. L. (1995). Psychophysically principled models of simple visual reaction time. *Psychological review*, *102*(3), 567–593.
Smith, P. L. (1998). Bloch's law predictions from diffusion process models of detection. *Australian Journal of Psychology*, *50*(3), 139–147.
Smith, P. L. (2000). Stochastic dynamic models of response time and accuracy: A foundational primer. *Journal of Mathematical Psychology*, *44*(3), 408–463.
Smith, P.L. From Poisson shot noise to the integrated Ornstein-Uhlenbeck process: Neurally principled models of information accumulation in decision-making and response time. *Journal of Mathematical Psychology*, in press (doi:10.1016/j.jmp.2009.12.002).
Stone, M. (1960). Models for choice reaction time. *Psychometrika*, *25*(3), 251–260.
Swensson, R. G. (1972). The elusive tradeoff: speed vs accuracy in visual discrimination tasks. *Perception & Psychophysics*, *12*, 16–32.
Uhlenbeck, G. E., & Ornstein, L. S. (1930). On the theory of the Brownian motion. *Physical Review*, *36*(5), 823–841.
Usher, M., & McClelland, J. L. (2001). On the time course of perceptual choice: the leaky competing accumulator model. *Psychological Review*, *108*(3), 550–592.
Usher, M., Tsetsos, K., & Teodorescu, A. (2009). Contrasting models of perceptual choice. In: *Annual meeting of the society for mathematical psychology*.
Vickers, D. (1970). Evidence for an accumulator model of psychophysical discrimination. *Ergonomics*, *13*(1), 37–58.
Wald, A. (1947). *Sequential analysis*. New York: Wiley.
Wallsten, T. S., & Barton, C. (1982). Processing probabilistic multidimensional information for decisions. *Journal of Experimental Psychology*, *8*(5), 361–384.
Yellott, J. I. (1971). Correction for fast guessing and the speed-accuracy tradeoff in choice reaction time. *Journal of Mathematical Psychology*, *8*(2), 159–199.
Zhang, J., & Bogacz, R. (2006). Optimal decision making with realistic bounds on neuronal activity. In: *15th annual computational neuroscience meeting*. Edinburgh.
Zhang, J., Bogacz, R., & Holmes, P. (2009). A comparison of bounded diffusion models for choice in time controlled tasks. *Journal of Mathematical Psychology*, *53*(4), 231–241.
Zhou, X., Wong-Lin, K.-F., & Holmes, P. (2009). Time-varying perturbations can distinguish among integrate-to-threshold models for perceptual decision-making in reaction time tasks. *Neural computation*, *21*(8), 2336–2362.